Electronic Supplementary Material (ESI) for Sustainable Energy & Fuels.

Supporting Information

Transcription methodology for rationally designed morphological complex metal oxides: A versatile strategy for improved electrocatalysis

*Sourav Bhowmick, Manoj Kumar Mohanta and Mohammad Qureshi**

Department of Chemistry, Indian Institute of Technology Guwahati, Assam- 781039, India.

*Corresponding author e-mail: mq@iitg.ac.in (M. Q.)

Material Characterization

X-ray diffraction measurement was accomplished using a Rigaku Smartlab X-ray diffractometer with copper K_α (λ=1.54 Å) as the source with 5 kW power. The XRD patterns were recorded from 2θ (10–80°) keeping the scan rate fix at 10° s^{-1}. To determine the morphological features of the samples, field emission scanning electron microscopy (FESEM) analysis was carried out using a Zeiss (model-Gemini and Sigma) instrument operated at 5kV. A CH Instruments model CHI760E, Inc., Austin, TX, was used to record the cyclic voltammetry (CV) and electrochemical impedance spectroscopy (EIS).

Electrochemical Measurements

Electrochemical measurements of the fabricated electrode were carried out on an electrochemical analyzer (model-CHI1120B) in a three-electrode system, using aqueous 1M NaOH as electrolyte (pH ~ 13), Ag/AgCl (saturated KCl) as reference electrode, graphite rod as counter electrode and the fabricated electrode as working electrode. Linear sweep voltammetry (LSV) was carried out from 0.1 V to 1 V vs. Ag/AgCl at a scan rate of 5 mV s^{-1}. Electrochemical impedance spectroscopy (EIS) measurements were carried out at open circuit potential vs. Ag/AgCl at frequency ranging from 0.1 Hz to 10^5 Hz. Cyclic voltammetry (CV) was performed between 0 V and 0.2 V vs. Ag/AgCl at scan rate ranging from 10 mV/s^{-1} to 2 mV/s^{-1}. All the potential applied using Ag/AgCl were converted to the reversible hydrogen electrode (RHE) scale by using the formula:

$$E_{RHE} = E_{Ag/AgCl} + 0.059pH + E^{0}_{Ag/AgCl} \quad \ldots (1)$$

E_{RHE} is the RHE potential, $E^{0}_{Ag/AgCl}$= 0.1976 V at 25 °C, $E_{Ag/AgCl}$ is the potential measured against the Ag/AgCl (saturated KCl) reference electrode, and pH is the pH of the electrolyte used.

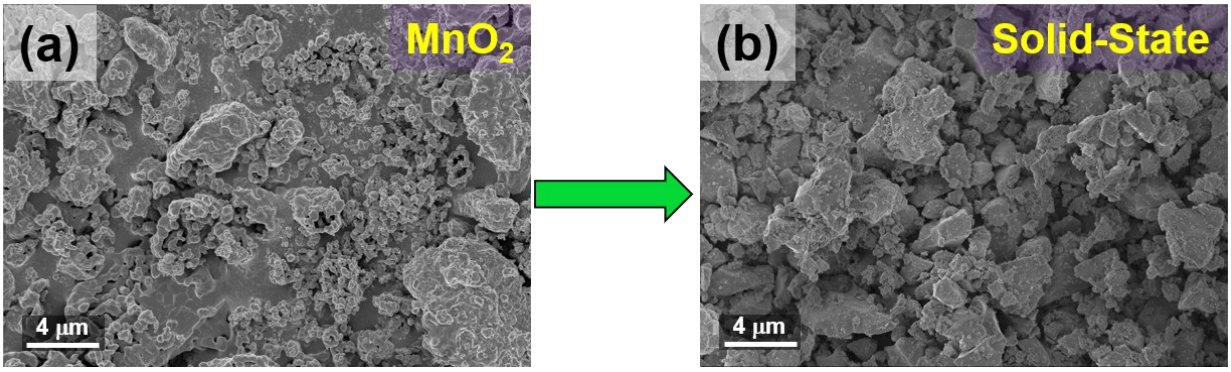

Figure S1. (a) FESEM image of commercial MnO_2 and (b) FESEM image of the LSMO synthesized using conventional solid-state method utilizing the commercial MnO_2

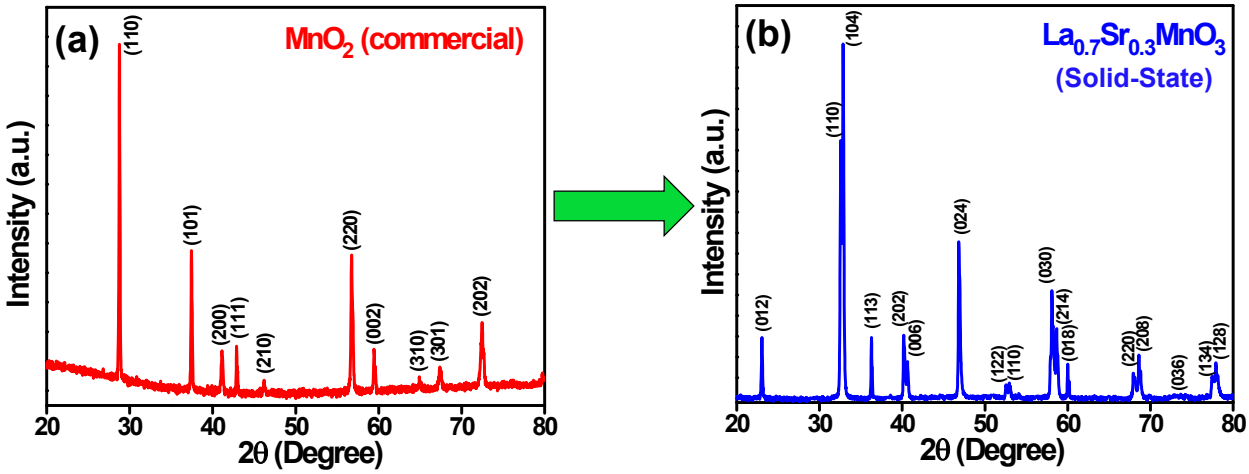

Figure S2. (a) PXRD plot of commercial MnO_2 and (b) PXRD of the synthesized LSMO using conventional solid-state method utilizing the commercial MnO_2 as Mn source

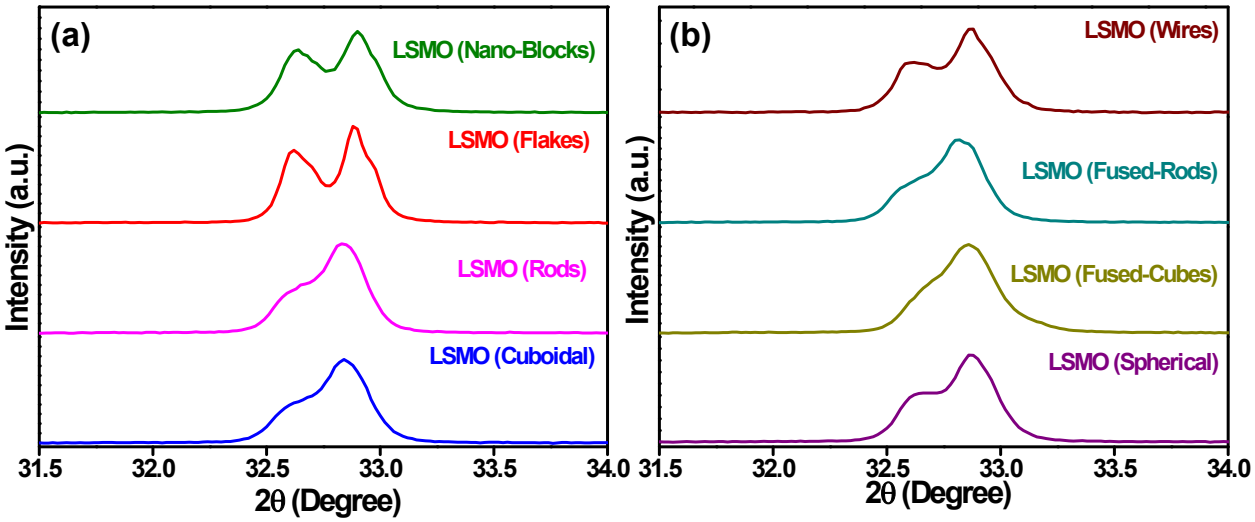

Figure S3. The enlarged XRD spectra at ~32° of the morphological LSMO demonstrating the pattern of the peak split

Rietveld refinement

The agreement of Rietveld refined data was evaluated with initial parameters in relation to the weighted and expected residual factors (R_{wp}, R_{ex}), and their ratio, corresponding to the goodness-of-fit (χ^2). The weighted-profile R value, R_{wp} was defined as

$$R_{wp} = \left[\Sigma_i W_i\{Y_i(obs) - Y_i(cal)\}^2 / \Sigma_i W_i\{Y_i(obs)\}^2\right]^{1/2} \quad \ldots (2)$$

where, Y_i (obs) was the observed intensity at step i, Y_i (cal) the calculated intensity, and W_i the weight. The expected R value (R_{exp}) was defined as

$$R_{exp} = \left[(N - P)\, \Sigma_i^N W_i\{Y_i(obs)\}^2\right]^{1/2} \quad \ldots (3)$$

where, N and P correspond to the number of observations and parameters respectively.

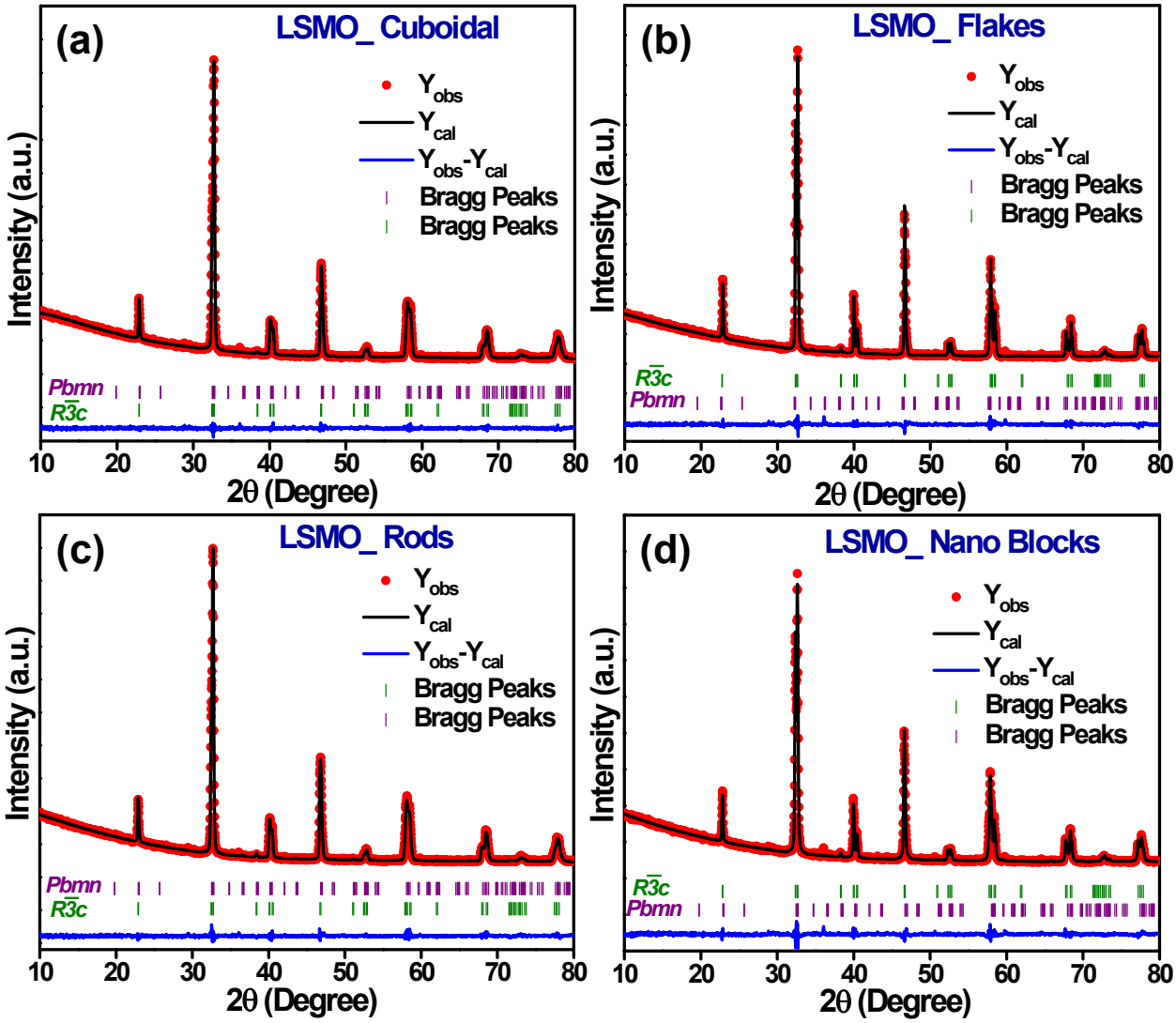

Figure S4. Rietveld refined XRD spectra of morphological LSMO synthesized from (a) cuboidal Mn_2O_3, (b) flake shaped KMn_8O_{16}, (c) rod shaped Mn_2O_3, and (d) nano-block shaped β- MnO_2 showing the presence of both rhombohedral and orthorhombic phases

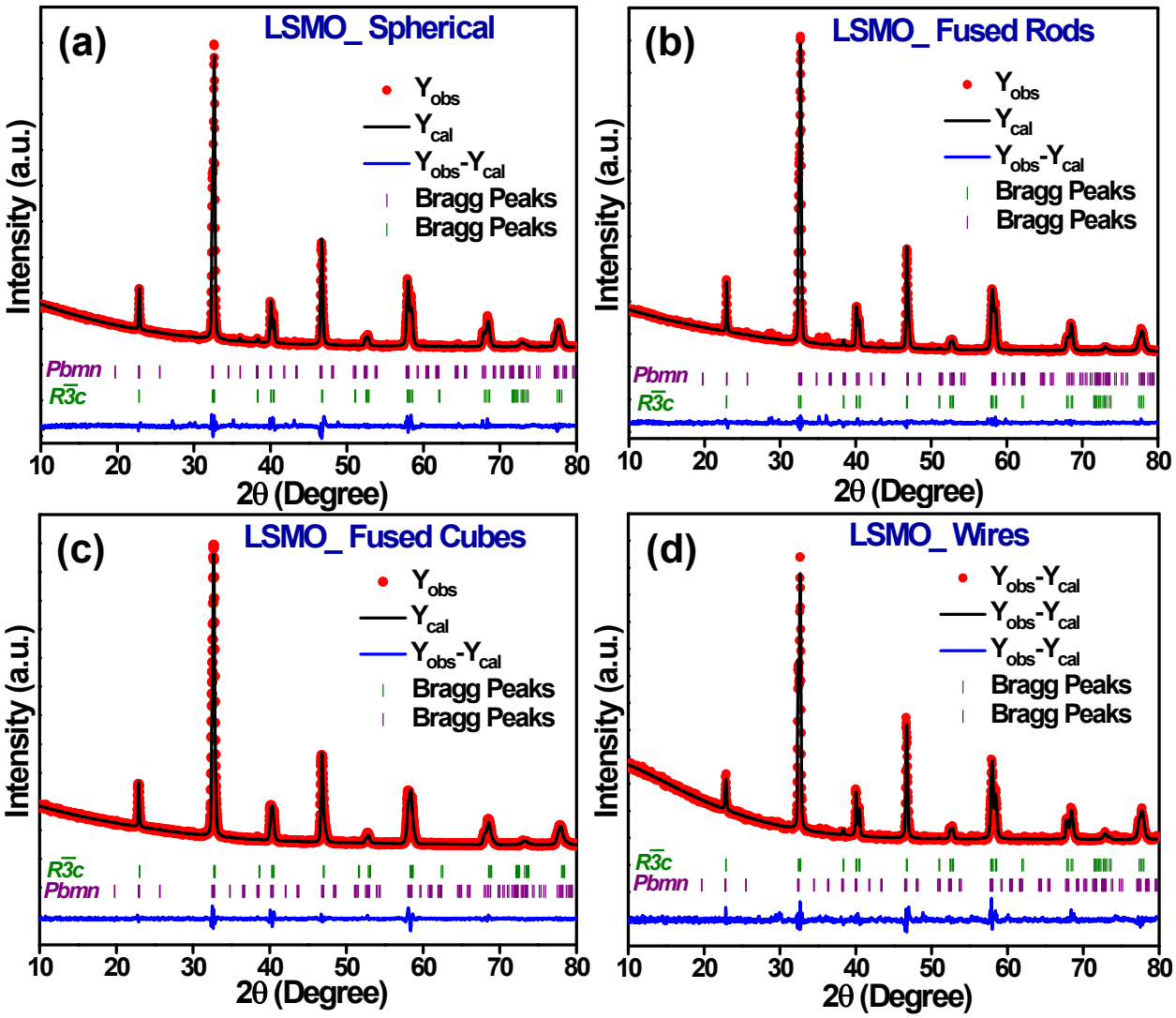

Figure S5. Rietveld refined XRD spectra of morphological LSMO synthesized from (a) spherical Mn_2O_3, (b) fused-rod shaped Mn_2O_3, (c) fused-cube shaped Mn_2O_3, and (d) wire shaped α-MnO_2 showing the presence of both orthorhombic and rhombohedral phases

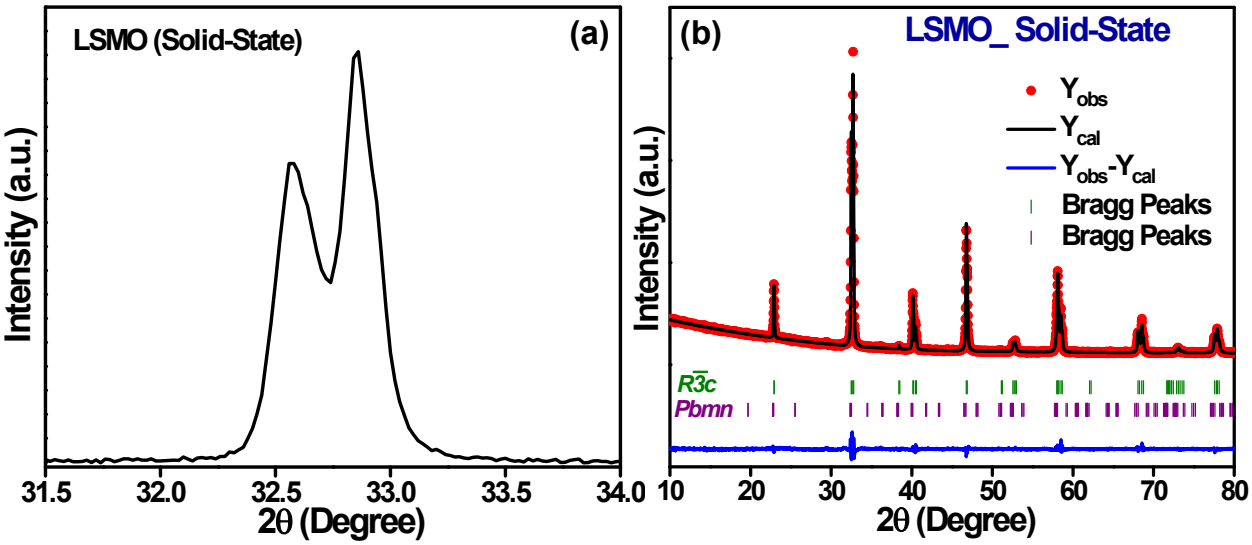

Figure S6. (a) The enlarged peak at ~32° for the conventional solid-state LSMO, and (b) Rietveld refined XRD spectra of LSMO synthesized from the commercial MnO_2

Table S1. Summary of the Rietveld refinement of the morphological LSMO and the conventional solid-state LSMO demonstrating the percentage of the formed mixed phases

Template MnO_x			**Transcripted $La_{0.7}Sr_{0.3}MnO_3$**		
Compound	**Morphology**	**Phase**	**Goodness-of-fit (χ^2)**	**Rhombohedral (R3c)**	**Orthorhombic (Pbmn)**
MnO_2	Non-uniform	Tetragonal	2.53	100%	0%
Mn_2O_3	Cuboidal	Cubic	1.73	43.97%	56.03%
KMn_8O_{16}	Flakes	Tetragonal	3.00	99.98%	0.02%
Mn_2O_3	Rods	Cubic	2.02	38.93%	61.07%
β-MnO_2	Nano-Blocks	Tetragonal	2.79	95.68%	4.32%
Mn_2O_3	Spherical	Cubic	3.30	69.87%	30.13%
Mn_2O_3	Fused-Rods	Cubic	2.44	33.50%	66.50%
Mn_2O_3	Fused-Cubes	Cubic	3.45	49.55%	50.45%
α-MnO_2	Wires	Tetragonal	2.58	99.99%	0.01%

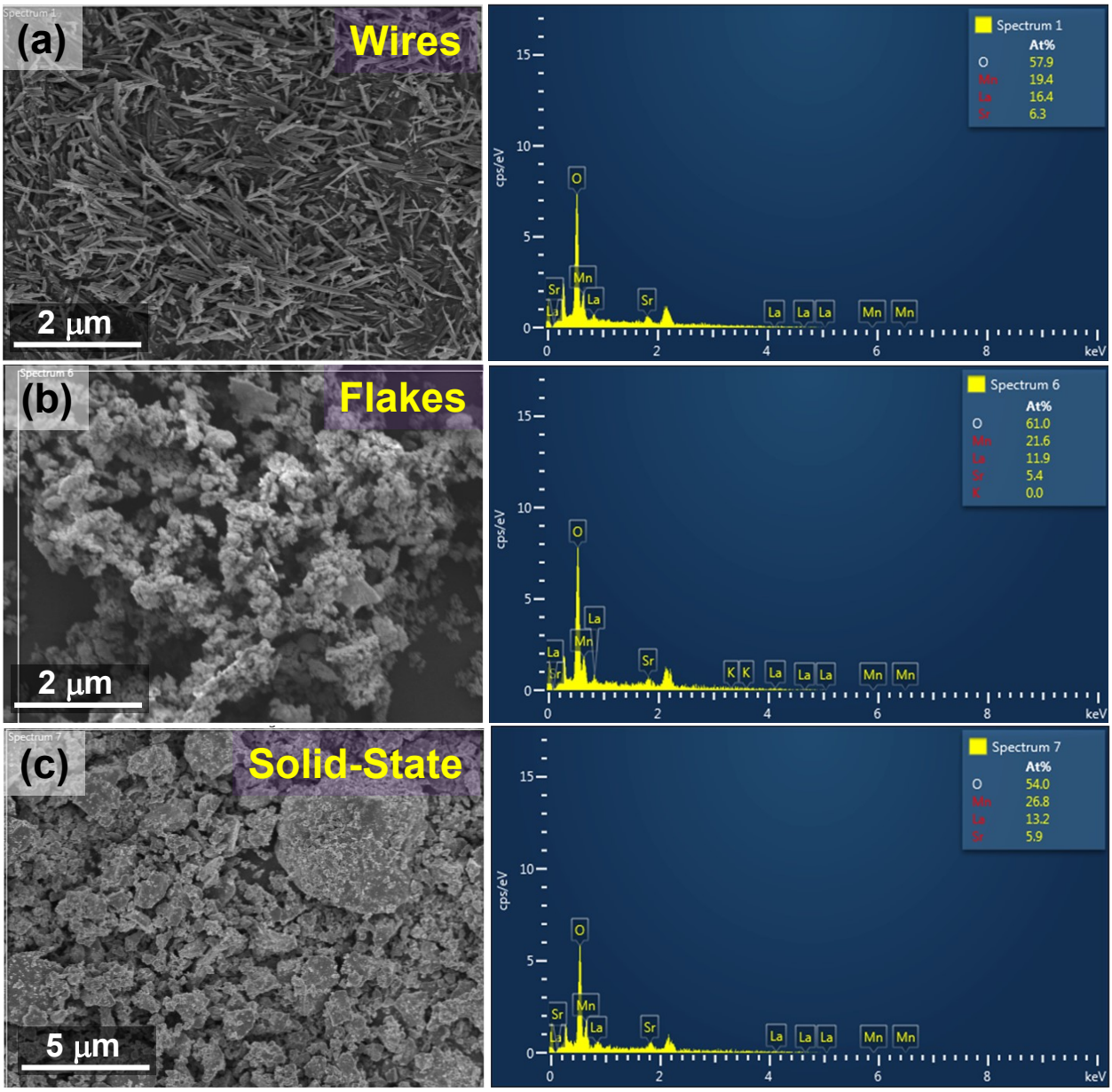

Figure S7. Energy dispersive X-Ray (EDX) analysis of (a) wire shaped **LSMO**, (b) flake shaped **LSMO**, and (c) conventional solid-state **LSMO** showing the atomic percentage of the constituent elements (lanthanum, strontium, manganese and oxygen) in the compound

From Figure S7, it is found that all the constituent elements are present in the wire shaped **LSMO** and conventional solid-state **LSMO**. The obtained atomic % of the elements were quantified and the obtained composition for wire shaped **LSMO** is $La_{0.79}Sr_{0.32}Mn_{0.98}O_{2.9}$, and for solid-state **LSMO** is $La_{0.66}Sr_{0.3}Mn_{1.3}O_{2.8}$. The obtained compositions are within the range of

experimental error, thus the desired doped lanthanum manganites were obtained for the morphological **LSMO**. Also, to confirm the presence of K species in flake shaped **LSMO** (derived from KMn_8O_{16} precursor), EDX technique was executed and the analysis showed no detectable presence of K species and the obtained composition is $La_{0.6}Sr_{0.27}Mn_{1.08}O_{3.05}$.

X-ray photoelectron spectroscopy (XPS) technique

To investigate the electronic structure and the chemical state of the constituent elements X-ray photoelectron spectroscopy (XPS) analysis was performed. Figure S8 depicts the XPS survey spectra confirming the presence of all the respective elements in the LSMO.

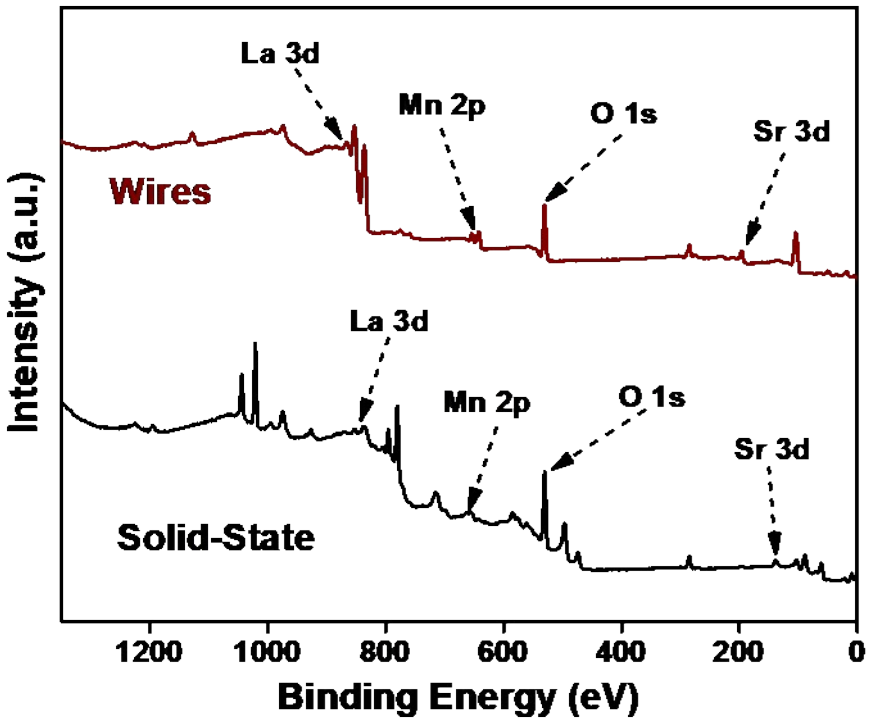

Figure S8. XPS survey spectra showing the presence of lanthanum, strontium, manganese, and oxygen in the both the wire-shaped and general solid-state LSMO

The XPS core-level spectra of La 3d (Figure S9(a)) has been de-convoluted into $3d_{5/2}$ and $3d_{3/2}$. The peaks for at 834.3 eV and 851.3 eV are due to La^{3+} while the peaks at 838.2 eV, 842.8

eV and 855 eV are satellite peaks. Similarly, for the wire-shaped LSMO the peaks at 834.5 eV and 851.2 eV are ascribed to La^{3+} while the peaks at 838.1 eV, 846.8 eV and 854.8 eV are satellite peaks.[S1,S2] Figure S9(b) shows the Mn 2p core-level spectra which is de-convoluted into $2p_{3/2}$ and $2p_{1/2}$ levels. The Mn $2p_{3/2}$ peak of general solid-state LSMO featuring at 641.6 eV, 653.4 eV and 643.3 eV, 654 eV can be attributed to Mn^{3+} and Mn^{4+}, respectively. The peak position at 646.6 eV is due to the satellite peak.[S1-S3] For the wire-shaped LSMO the peaks at 641.5 eV, 653.2 eV and 643.5 eV, 654.2 eV corresponds to Mn^{3+} and Mn^{4+}, respectively, with the satellite peak at 647.3 eV. Figure S9(c) shows the O1s core-level spectra for general solid-state and wire-shaped LSMO. The peaks at 529.6 eV and 529.5 eV, respectively, are due to the lattice oxygen O^{2-} (O_L) associated with Mn atom. The peaks at 531.3 eV and 531.1 eV, respectively, corresponds to the surface adsorbed oxygen species (O_{ads}), like O^-, O^{2-}, or O_2^{2-}. While the respective peaks at 532.9 eV and 532.4 eV corresponds to hydroxyl groups (O_{O-H}) weakly bound to the surface.[S1-S3] The increase in the area of the peaks for O_{ads} and O_{O-H} of the wire-shaped LSMO may be due to the enhanced surface area of the compound. In Figure S9(d) the XPS spectra for Sr 3d has been de-convoluted into respective $3d_{5/2}$ and $3d_{3/2}$ with peak ratio of 3:2. The peaks at 132.9 eV, 132.3 eV and 133.8 eV, 133.5 eV are assigned to Sr^{2+} in the bulk and surface of the material, respectively for general solid-state and wire-shaped LSMO.[S1,S2]

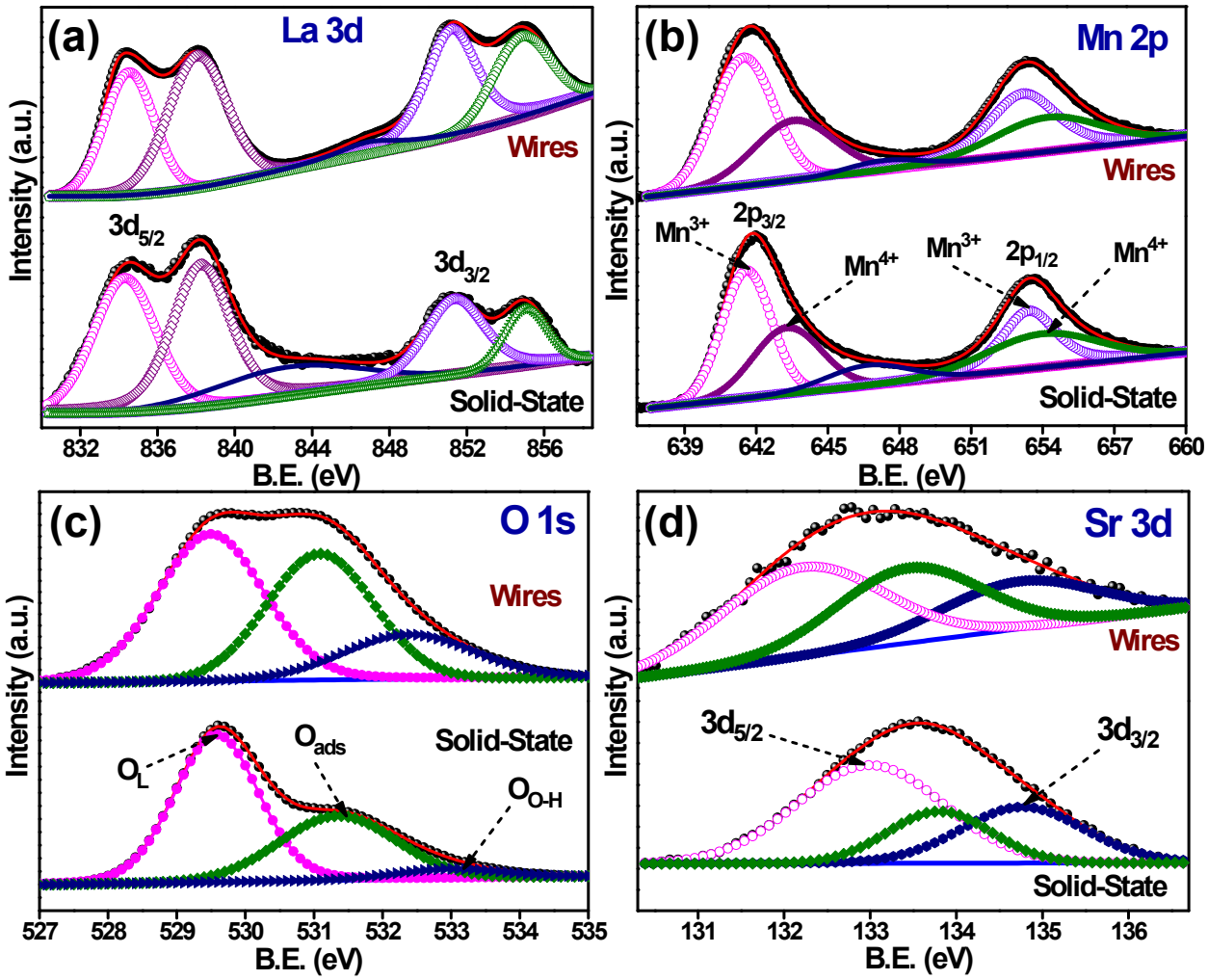

Figure S9. The core-level XPS spectra of (a) La 3d, (b) Mn 2p, (c) O 1s, and (d) Sr 3d of wire-shaped and conventional solid-state LSMO

Determination of electrochemical active surface area (ECSA)

ECSA is used to predict the activity trends when a set of similar catalytic materials is studied or to determine the reasons behind a difference in the activities of similar catalysts in the same study. ECSA can be calculated from the measurement of double-layer capacitance (C_{dl}) value for the respective catalysts using cyclic voltammetry (CV) technique. ECSA is proportional to the C_{dl} value as follows,

$$ECSA = C_{dl} \times C_S \quad \ldots (4)$$

Where, C_S is the specific capacitance of the material and C_{dl} value is obtained from the CV plots at non-Faradaic region. The value is equal to the half of the slope value obtained from the plot of the difference in current density between the anodic and cathodic sweeps ($J_{anodic} - J_{cathodic}$) at a particular potential as a function of the scan rate.[S1,S4]

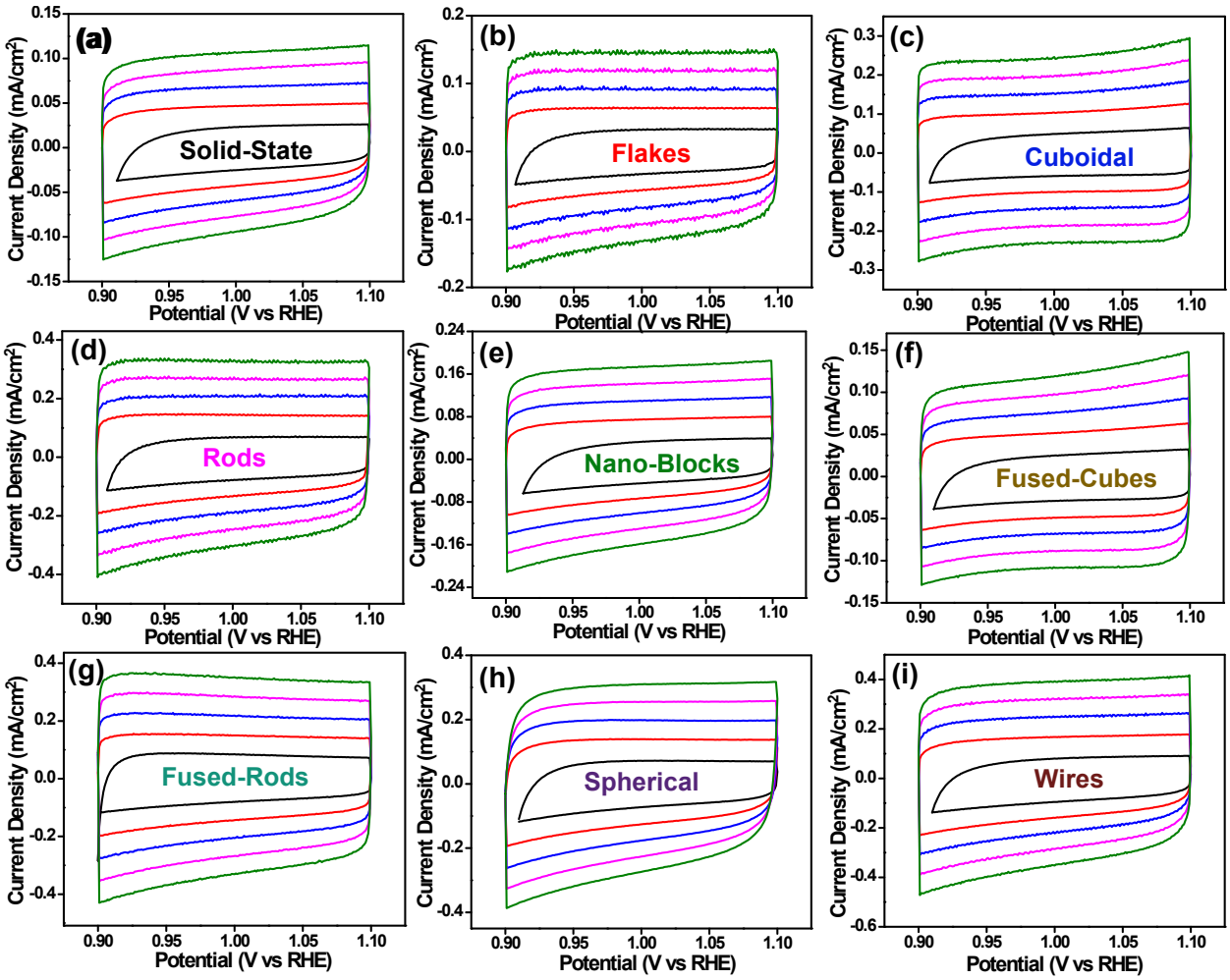

Figure S10. Cyclic Voltammograms of the different LSMO measured in the non-Faradaic region (0.9 V to 1.1 V vs. RHE) at scan rates of 2, 4, 6, 8 and 10 mV/s

Calculation of turnover frequency (TOF)

Turnover frequency (TOF) was calculated as:

$$TOF = \frac{J \times A}{4 \times n \times F} \quad \ldots (5)$$

where **J** is the current density at a given potential, **A** is the surface area of the electrode (1 cm^2 for the LSMO electrode), 4 is the number of electrons transferred in the OER, n is the number of moles of all metal ions available for the OER (including La, Sr and Mn), and F is Faraday's constant (96485 C mol^{-1}).[S5,S6]

References:

S1. S. Bhowmick, A. Dhankhar, T. K. Sahu, R. Jena, D. Gogoi, N. R. Peela, S. Ardo and M. Qureshi, *ACS Appl. Energy Mater.*, 2020, **3**, 1279–1285.

S2. A. Giri, N. Goswami, M. S. Bootharaju, P. L. Xavier, R. John, N. T. K. Thanh, T. Pradeep, B. Ghosh, A. K. Raychaudhuri and S. K. Pal, *J. Phys. Chem. C*, 2012, **116**, 25623–25629.

S3. W. Xia, Z. Pei, K. Leng and X. Zhu, *Nanoscale Res. Lett.*, 2020, **15**, 9.

S4. S. Anantharaj, S. R. Ede, K. Karthick, S. Sam Sankar, K. Sangeetha, P. E. Karthik and Subrata Kundu, *Energy Environ. Sci.*, 2018, **11**, 744–771.

S5. G. Li, S. Li, J. Ge, C. Liu and W. Xing, *J. Mater. Chem. A*, 2017, **5**, 17221–17229.

S6. T. Zhou, Z. Cao, P. Zhang, H. Ma, Z. Gao, H. Wang, Y. Lu, J. He and Y. Zhao, *Sci. Rep.*, 2017, **7**, 46154.